Phenomenological description and Monte Carlo simulation of multiparticle production in high-energy NN and πN collisions

V. S. Barashenkov and N. V. Slavin

Joint Institute for Nuclear Research, Dubna

Fiz. Elem. Chastits At. Yadra **15**, 997–1031 (September–October 1984)

Phenomenological expressions are obtained for the differential single-particle inclusive cross sections for the production of nucleons and pions in inelastic NN and πN collisions. These expressions describe the known experimental data in a wide range of the kinematic variables at energies from 5 to 5×10^3 GeV. The Monte Carlo method makes it possible to simulate individual inelastic collision events and to analyze the properties of the leading particles.

INTRODUCTION

To analyze the mechanisms of interaction of hadrons with nuclei, design radiation shielding, estimate the intensity of beams of secondary particles in accelerators, and for many other theoretical and applied problems it is necessary to have detailed information about the multiplicity, emission angles, energies, and other characteristics of the secondary particles in inelastic NN and πN collisions. In the literature there is a large amount of experimental data on these quantities, but the information is, as a rule, widely dispersed and refers to individual, frequently widely separated regions of the kinematic variables; in a number of cases, different normalizations and different variables are used. Interpolation of the known experimental data to the intermediate regions and their extrapolation usually involve considerable difficulties, especially since for some problems (for example, the calculation of intranuclear cascades or the propagation of particle beams in media) detailed data in a very wide energy interval are needed, and the storage of such extensive numerical information in a computer presents difficulties. In all cases, it is important to have a unified and compact analytic representation of the data.

Many different models of inelastic particle collisions at high energies have been considered in the literature: the statistical and hydrodynamic approaches, the diagrammatic and Regge techniques for the calculation of peripheral interactions, and so forth. These models can be successfully used to describe individual aspects of the phenomenon. However, in practice this is frequently insufficient, the models being in addition very complicated for calculations. Therefore, in many cases one must have recourse to various phenomenological approximations of the experimental data, the theoretical models being used only to "suggest" a particular choice of the approximating expressions.

In Refs. 1 and 2, a statistical, Monte Carlo approximation of multiparticle production in NN and πN collisions was developed on the basis of the assumption that the energy spectra of the secondary particles depend very weakly on their emission angle. Such an approach, especially if one introduces an additional rejection of simulated events on the basis of the experimental distribution of the transverse momentum, makes it possible to achieve agreement with the experiments in a wide range of energies from a few hundred mega-electron-volts to 5–10 GeV,[1,2] i.e., at energies at which the so-called leading particles are not yet clearly distinguished by their energy.[1)] It is possible not only to calculate the mean angular and energy distributions of the secondary particles but also to recover (simulate) individual events ("stars") of an inelastic collision in such a way that in each of them the characteristics of the produced particles satisfy the energy–momentum conservation laws. A much more general approach to the quantitative analysis of multiparticle production was made possible after Logunov, Feynman, Yang, and their collaborators proposed the concept of inclusive reactions, and Mueller introduced for them an optical theorem (see Refs. 3 and 4, in which a detailed bibliography can be found). Although this theorem relates the amplitude of an inclusive reaction only to three-particle elastic scattering, which cannot be realized in practice, for the theoretical analysis of this—much simpler—process Regge phenomenology can be used.

Many authors have shown that by an appropriate choice of the parameters it is indeed possible to achieve a good description of the experimental data down to individual reaction channels,[4,5] though in each case the analysis is, as a rule, restricted to a narrow region of the kinematic variables, basically near $x\sim\pm1$ and $T\gg10$GeV.[2)] However, if the expressions suggested by Mueller's theorem are used only as an analytic "skeleton" with coefficients chosen by comparison with experiment—possibly with some additional phenomenological terms needed for smooth "matching" of kinematic regions that differ in their physical nature—one can attempt to find an approximation compact in form and valid for a wide interval of the independent variables $s, x, p_\perp$. It is to be borne in mind that since the approximating expressions have a theoretical basis, they are not merely a phenomenological interpolation between experimental points but possess a certain heuristic value, making it possible to go beyond the known experimental data.

[1)] In the calculation of the mean values, the agreement with experiment is maintained even at energy 10–20 GeV.[2]

[2)] In all that follows, we shall consider the center-of-mass system and use the standard notation: s is the square of the total energy of the colliding particles, $p_\parallel$ and $p_\perp$ are the longitudinal and transverse components of the momentum of a secondary particle in this system, $E=\mathscr{T}+M=(p_\parallel^2+p_\perp^2+M^2)^{1/2}$ and $\mathscr{T}$ are the total energy and the kinetic energy of the considered secondary particle, $x=2p_\parallel^*s^{-1/2}$, and T is the kinetic energy of the incident particle in the laboratory system.

 0090-4759/84/050446-18$04.40

One of the main difficulties that arise in the construction of approximating expressions is that the currently known experimental data do not yet permit the determination of the numerical coefficients with equal accuracy for all types of reactions involving different charges of the primary and secondary particles. For example, the spectra of neutrons in pp collisions have as yet been very poorly investigated; there are very few data for pn interactions, especially for the secondary neutrons, and there are almost no data on the production of neutral particles in πN collisions. In such cases, it is necessary to modify the expressions obtained for particles of a different charge, and this can introduce certain errors in the absolute value of the particle-production cross sections and can significantly distort the form of the differential inclusive distributions $Ed^3\sigma(x, p_\perp, s)/dp^3$, particularly at large x and $p_\perp$.

Nevertheless, for the tasks listed above the accuracy of the phenomenological expressions for $Ed^3\sigma/dp^3$ is quite acceptable, since large momenta are important primarily only for the leading particles, whose distribution can be approximated fairly accurately; with regard to the remaining particles, they have large values of x and $p_\perp$ comparatively seldom. If particle collisions are simulated by the Monte Carlo method, the errors in the absolute value of the cross sections $d^3\sigma/dp^3$ are also unimportant, since the multiplicity of the secondaries, their energies, and emission angles can be determined by means of the relative—for example, normalized to unity—differential distributions (see Ref. 2 and Sec. 6 below).

It should be noted that because the experimental cross sections $Ed^3\sigma/dp^3$ used in the selection of the coefficients in the approximating expressions are not sufficiently accurate it is frequently found that an approximation which gives a good description of the differential distributions leads to values of the mean energy $\langle \mathscr{T} \rangle$ of the produced particles, their mean transverse momentum $\langle p_\perp \rangle$, and other integral characteristics in poor agreement with experiment (differing by factors up to 1.5–2). At the same time, the accuracy of the approximating expressions is greatly improved if these expressions are chosen subject to the condition of good agreement of the calculated integral quantities with the results of the measurements. The approximations given below were obtained by taking into account this requirement.

Much of our paper is devoted to the approximation of the single-particle inclusive cross sections $Ed^3\sigma/dp^3$ and integral quantities associated with them (mean multiplicity, inelasticity coefficients, etc.) and comparison of them with experiment. After this, we consider how the Monte Carlo method and the known expressions for $Ed^3\sigma/dp^3$ can be used to recover detailed characteristics of individual inelastic NN and πN collisions. The discussion covers a wide energy interval from $T \geqslant 5$ to $T \simeq 5 \times 10^3$ GeV. At lower energies, the characteristics of the secondary nucleons can be determined by using the well-developed Monte Carlo methods and approximating expressions based on resonance models (see Ref. 2, in which further bibliography can be found). At energies above a few thousand giga-electron-volts, where there are only scattered and inaccurate cosmic-ray experimental data, our expressions with experimentally determined coefficients become very approximate. However, because of the lack of experimental information even such approximate expressions have here considerable interest.

It is very important to bear in mind that the considered approximation of the experimental data is valid only sufficiently far from the interaction point, i.e., where all the produced resonance states have completely decayed into pions and nucleons.

1. CHOICE OF APPROXIMATING EXPRESSIONS

Following the results of the Regge–Mueller analysis (see Fig. 1 and the review of Ref. 4), we shall assume that in the fragmentation region $|x| \sim 1$, where elastic three-particle scattering is determined mainly by three-Reggeon processes, the cross section of the inclusive reaction $a + b \to c + \ldots$ has the form

$$\left(E\frac{d^3\sigma}{dp^3}\right)_{\text{frag}} = \sum_{i=1}^{4} G_i e^{R_i t}(1-|x|)^{\beta_i - \gamma_i t}\left(\frac{s}{s_0}\right)^{\alpha_i} + G e^{Rt}(1-|x|)^{1-\gamma t}\,|t|/(M_\pi^2 - t)^2. \quad (1)$$

Here, $G_i \exp(R_i t)$ are vertex functions, including signature factors; $\alpha_i, \beta_i, \gamma_i, \gamma$ are the parameters of the Regge trajectories $a_i(t) = a_i(0) + a_i'(0)t$, where the four-dimensional momentum transfer from the target particle b to the produced particle c is $t = -(p_\perp^2/|x|) - (1-|x|)(M_c^2/|x| - M_a^2)$, in which M_a and M_c are the masses of the primary particle and the secondary particle, and M_π is the pion mass; $s_0 = 1$ GeV^2. The first term in this expression is determined by the three-Reggeon process with participation of the Pomeron and "effective" Regge trajectories, and the second term is determined by the exchange process with participation of a pion Regge trajectory. Such an approximation has been used by many authors and has proved to be very effective.

In the central region of x values, in which the decisive contribution to the elastic three-particle scattering is made by pole diagrams of the type C in Fig. 1, the cross section of the inclusive reaction has the structure

$$\left(E\frac{d^3\sigma}{dp^3}\right)_c = (A + B|x| + C|x|^{-1})/(p_\perp^2 + \mu^2)^D. \quad (2)$$

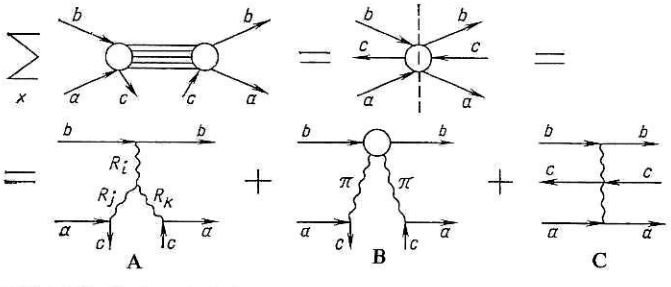

FIG. 1. Mueller's optical theorem for the inclusive process $a + b \to c + X$. By means of the unitarity condition, the sum of the amplitudes of the inclusive reactions with different systems (groups of particles) X is "convoluted" into the amplitude of elastic three-particle scattering, which, in its turn, can be represented in the form of a sum of the amplitudes A, B, C with exchange of Regge trajectories: A, three-Reggeon exchange in the fragmentation region; B pion exchange in the fragmentation region; C, Reggeon exchange in the central region of x values.

TABLE I. Values of coefficients for calculating the spectra of conserved and nonconserved nucleons for $|x| \leqslant 0.7$.

Reaction	a, mb/GeV^2	b	c	d	f, $(\text{GeV}/c)^{-2}$	g	μ^2, $(\text{GeV}/c)^2$	u, mb/GeV^2	v
$pp \to p+\ldots$	100	9,4	−0,06	6,43	0,21	1.5	1,81	230	−1
$x<0$	6.1	3.6	−0,01	4,9	1,0	2.7	1,36	210	−1
$pn \to p+\ldots$									
$x>0$	95	8.5	−0,06	6.43	0,45	1.4	1.84	210	−1
$pp \to n+\ldots$	13	0,35	0,17	5,5	1,2	−0.4	1,25	210	−1

where the coefficients A, B, C, D are functions of the variables $p_\perp$ and s.

We shall consider separately the properties of the "conserved" particles c, when particle c is identical to one of the primary particles (i.e., $c \equiv a$ or $c \equiv b$) and is emitted into the same hemisphere as this primary particle, and the properties of all the remaining "nonconserved" particles. The physical justification for this distinction is that on the average the former have a much higher energy than the latter and are collimated in a region of smaller angles.[3)] The conserved particles can be produced both in fragmentation and in nonfragmentation ("central") processes. In the production of the nonconserved particles the central processes play a much more important part.

For the conserved particles, the expression (2) can be conveniently parametrized in the form

$$\left(E\frac{d^3\sigma}{dp^3}\right)_{\text{c.c.}} = a\,(1+b\,|x|\,s^{c-x_\perp s^{0,27}})\,(1-|x|)^{fp_\perp^2} e^{g|x|}\,(p_\perp^2+\mu^2)^d, \tag{3}$$

with coefficients that do not depend on s, $p_\perp$, and x.

For the nonconserved particles, we write the expression (2) in the form of two terms:

$$\left(E\frac{d^3\sigma}{dp^3}\right)_{\text{c.nc.}} = a\,(1-|x|)^b \times \times [s^{c(1+|x|)}p_\perp^2 e^{-1,3p_\perp^2}/(p_\perp^2+1)^4 + ds^{f(1-|x|)}e^{-hp_\perp^2}/(|x|+1)^g]. \tag{4}$$

Here, $s = s/s_0$, $p_\perp = p_\perp/p_{\perp 0}$, where $p_{\perp 0} = 1\,\text{GeV}/c$.

The expressions (1)–(3) can be made the basis of an approximation of the experimental data. However, calculations show that for these expressions it is not possible to choose coefficients valid in a wide range of x, $p_\perp$, s values. This is due to the fact that the expressions (1)–(3) relate to limiting cases and are very inaccurate in the intermediate region. To describe this region, it is necessary to include an additional phenomenological term making it possible to "match" continuously the fragmentation and nonfragmentation processes. We choose this term in the form

$$\left(E\frac{d^3\sigma}{dp^3}\right)_{\text{add}} = us^v\,(1-|x|)\,e^{-5p_\perp^2} \tag{5}$$

with constant u and v.

The coefficients in the approximating expressions must be chosen for each particular reaction.

2. THE REACTION $N+N \to N+\ldots$

We write the inclusive cross section (in mb/(GeV$^2/c^3$)) for production of conserved particles in the following form, which is valid in a wide range of values of the kinematic variables[4)]:

$$E\frac{d^3\sigma(x,\,p_\perp,\,s)}{dp^3} = \begin{cases} (Ed^3\sigma/dp^3)\,\text{c.c.} + (Ed^3\sigma/dp^3)_{\text{add}}, & \text{if } 0 \leqslant |x| < 0.7; \\ (Ed^3\sigma/dp^3)_{\text{frag}}, & \text{if } 0.7 \leqslant |x| \leqslant x_{\max}. \end{cases} \tag{6}$$

In pp and nn collisions, in which the conserved particle is, respectively, a proton and a neutron, the particle distributions in the regions of positive and negative x are symmetric about $x = 0$. Such symmetry is absent for pn interactions, in which a proton for $x > 0$ and a neutron for $x < 0$ are assumed to be conserved particles (in an np interaction, the sign of x is reversed).[5)]

The expression (6) is also valid for the description of the spectra of nonconserved nucleons in reactions with charge exchange of the incident particles: neutrons in pp interactions, protons with $x < 0$ and neutrons with $x > 0$ in pn interactions (and the corresponding particles) in the charge-symmetric nn and np collisions). There is a difference from the case of conserved particles only in the values of the coefficients.

In Tables I and II, we give the values of the coefficients chosen on the basis of the known experimental data at energies $T \gtrsim 5$ GeV.[6)] As mentioned in the Introduction, not only

[3)] A "conserved" particle should not be confused with a "leading" particle, which carries away a large fraction of the interaction energy. Among the leading particles, there is a certain fraction of nonconserved particles (see Sec. 5).

[4)] Instead of the distribution with respect to the variables x and $p_\perp$, it is frequently important to know the energy spectrum of the secondary particles for a given emission angle of the particles: $d^2\sigma(\mathcal{T}, \cos\theta, s)/d\mathcal{T}\,d\cos\theta$. This spectrum is obtained by multiplying the expression (6) by the factor $p = 4\pi\mathcal{T}^{1/2}(\mathcal{T}+2M)^{1/2}$ and substituting the values $x = 2ps^{-1/2}\cos\theta$ and $p_\perp = p\sin\theta$.

[5)] It follows from kinematic considerations that in the general case the cross sections for the production of conserved particles b in the reaction $a+b \to b+\ldots$ and a in the reaction $a+b \to a+\ldots$ are described by the same expression (6). [The emission angles of particles a and b are related by $\theta_b = \pi - \theta_a$. A change in the sign of x does not affect the form of the expression (6), where $|x|$ is used.] If the masses of particles a and b are different, the value of M_c must be changed in this expression accordingly.

[6)] The coefficients for the description of the particles in nn and np reactions are obtained on the basis of charge symmetry.

TABLE II. Values of coefficients for calculating the spectra of conserved and nonconserved nucleons for $|x| \geqslant 0.7$.

Coefficients that are the same for all reactions				For $pp \to p + \ldots$		For $pn \to p + \ldots$,			For $pp \to n + \ldots$	
						$x<0$		$x>0$		
G, mb/GeV^2				19		14		23	3.8	
R, $(\text{GeV}/c)^{-2}$				4.3		0.01		5.6	0.23	
γ, $(\text{GeV}/c)^{-2}$				0.6		1.36		1.2	1.62	
i	α_i	β_i	γ_i, $(\text{GeV}/c)^{-2}$	G_i, mb/GeV^2	R_i, $(\text{GeV}/c)^{-2}$	G_i, mb/GeV^2		R_i, $(\text{GeV}/c)^{-2}$	G_i, mb/GeV^2	R_i, $(\text{GeV}/c)^{-2}$
						$x<0$	$x>0$	$x<0$ $x>0$		
1	0	0	1.5	3.3	−0.38	6.5	5.7	3 0.07	—	—
2	0	−0.5	0.85	9	6.5	—	1	— 10	0.007	0.45
3	−0.5	−0.5	1.5	57	3.6	—	24	— 1.4	5.1	4.1
4	0	−1	0.2	0.2	1.5	—	0.07	— 1.3	—	—

the differential distributions but also the experimental data for the integral characteristics of the produced particles were used. Figures 2 and 3 illustrate the accuracy of the approximation of the experimental data for the conserved particles; Figs. 4 and 5 give the corresponding data for nonconserved particles.

The theoretical curves reproduce well the main features of the inclusive cross sections for production of nucleons, namely, the slow variation of the cross sections in the central region of x values, their rapid increase at $|x| \sim 1$ for conserved particles and decrease in the case of charge-exchange reactions, and the very rapid decrease in the probability of production of nucleons with large transverse momenta. In the case of pp interactions, there is good qualitative agreement with the experiments in the region $x > 0.5$. At smaller values of x, where at present there are only a few scattered experimental data and the coefficients of the expressions (6) are determined mainly on the basis of the known integral characteristics, the accuracy of the approximation is somewhat less good. The approximation of the spectra of a nonconserved neutron in pp collisions does not go outside the average experimental errors.

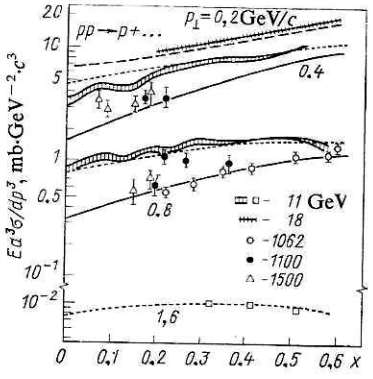

FIG. 2. Differential distributions of secondary protons in inelastic pp collisions for the region $x \leqslant 0.6$. The dotted curves are the calculation for $T = 10$ GeV, the broken curves for $T = 18$ GeV, and the continuous curves for $T = 10^3$ GeV.[7]

The case of the pn reaction is more difficult because of the sparsity of experimental information. The values of the coefficients in Tables I and II give the best agreement with experiment (Fig. 6), but more detailed measurements may require more accurate determination of these coefficients.

The mean multiplicity of the produced particles c is related to the inclusive cross section by

$$\langle n_c \rangle = \sigma_{\text{in}}^{-1} \int d^3\sigma_c = \sigma_{\text{in}}^{-1} \int \left(E \frac{d^3\sigma_c}{dp^3} \right) \frac{d^3p}{E}, \tag{7}$$

where σ_{in} is the total experimental inelastic interaction cross section. Use of the inclusive cross section (6) leads to the conclusion that in the region $T \gtrsim 5$ GeV the proton and neutron multiplicities remain practically constant (in pp collisions $\langle n_p \rangle \simeq 1.4$, $\langle n_n \rangle \simeq 0.6$). This agrees well with experiment (Fig. 7) and indicates a low probability for production

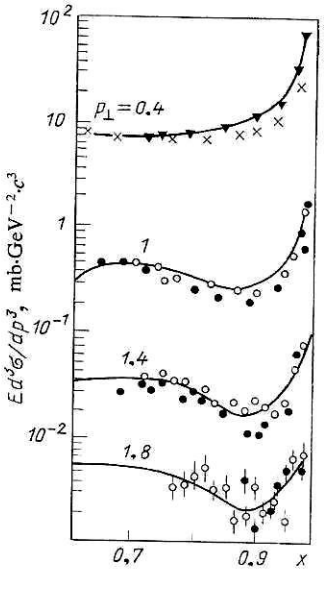

FIG. 3. Differential distributions of secondary protons in inelastic pp collisions for the region $x \geqslant 0.6$. The curves are the calculation for $T = 10^3$ GeV; the crosses, black triangles, black circles, and open circles are the experimental points of Refs 8 and 9 for $T = 385$, 659, 1062, and 1482 GeV, respectively.

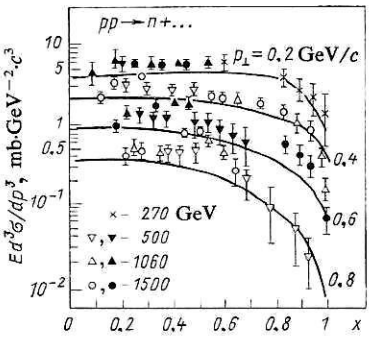

FIG. 4. Differential distributions of neutrons in pp interactions. The curves are the calculation for $T = 10^3$ GeV; the experimental points are taken from Ref. 10.

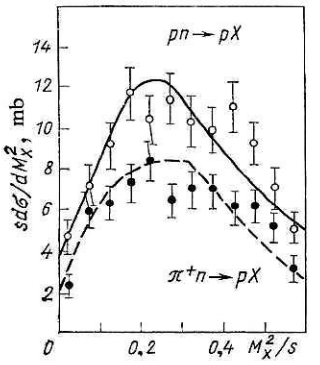

FIG. 6. Integrated cross section of the reaction $p(\pi^+)n \to p + \ldots$ as a function of the variable M_X^2/s for the region $|t| < 1$ (GeV/c)^2 and energy $T = 100$ GeV. The experimental points are taken from Ref. 13.

of nucleon–antinucleon pairs ($\langle n_p^- \rangle \sim 0.1$).

Statistical arguments based on isotopic invariance are often invoked to assert that if the number of secondaries is large, then $\langle n_p \rangle \simeq \langle n_n \rangle$ irrespective of the charge of the colliding nucleons. The given data show that in pp collisions the mean proton and neutron multiplicities remain different even at very high energies. Only in the case of pn interactions can one speak of equality of $\langle n_p \rangle$ and $\langle n_n \rangle$.

Table III gives the mean transverse momenta of the protons in pp collisions:

$$\langle p_\perp (s) \rangle = \sigma [p_\perp; s]/\sigma [1; s], \tag{8}$$

where the functional σ of the kinematic variable z (in the given case, $z = p_\perp$) is given by

$$\sigma [z; s] = \frac{\pi}{2} \int_{-x_{\max}}^{+x_{\max}} dx \int_0^{p_{\perp\max}^2 (x)} E \frac{d^3\sigma (x, p_\perp, s)}{dp^3} \frac{z (x, p_\perp, s)\, dp_\perp^2}{(x^2 s/4 + p_\perp^2 + M_c^2)^{1/2}}, \tag{9}$$

$$\left.\begin{aligned} x_{\max} &= 2s^{-1/2} (E_{\max}^2 - M_c^2)^{1/2}, \\ p_{\perp\max}^2 (x) &= E_{\max}^2 - x^2 s/4 - M_c^2 \end{aligned}\right\} \tag{10}$$

are the maximal values of the variable x and the square of the proton transverse momentum $p_\perp$.

$$E_{\max} = (s + M_c - M_x^2)/2s^{1/2}$$

is the maximal possible energy of a secondary particle, M_c is the mass of the considered secondary particle ($M_c = M_p$ in the given case), and M_x is the minimal mass of the produced particles of the system X in the inclusive reaction $a + b \to c + X$.[6]

The calculated $\langle p_\perp \rangle$ are close to the experimental values, which are about 0.4 GeV/c in the region $T \simeq 5$–30 GeV and increase to 0.45 GeV/c at $T \simeq 10^3$ GeV.

Compared with the protons, the means transverse momenta of the neutrons produced in pp collisions are several percent greater, although it is difficult to insist on this difference in view of the errors of the employed approximations.

Table III also gives the mean kinetic energy of a proton in the center-of-mass system.

$$\langle \mathcal{T}_p (s) \rangle = \sigma [E; s]/\sigma [1; s] - M_p, \tag{11}$$

and the mean fraction of the energy carried away by it:

$$\langle K_p (s) \rangle = s^{-1/2} \{ \langle \mathcal{T}_p (s) \rangle + M_p \}. \tag{12}$$

At $T \simeq 10$ GeV, the value of $\langle \mathcal{T}_p \rangle$ is close to the experimental value 0.6 GeV (Refs. 35 and 36) and then increases some-

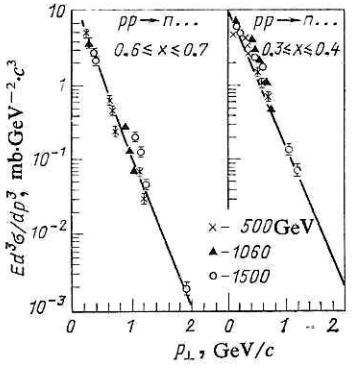

FIG. 5. Distribution of the neutrons in pp interactions with respect to the magnitude of their transverse momentum. The curves are the calculation for $T = 10^3$ GeV. Next to the curves we have given the ranges of x values to which the experimental points correspond.[10] (The calculation was made for the corresponding mean values.)

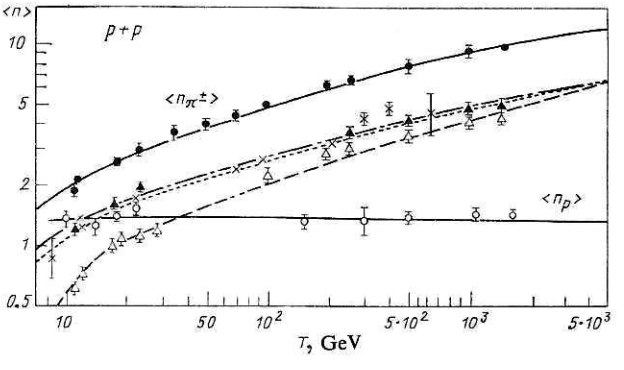

FIG. 7. Mean multiplicity of particles in inelastic pp collisions. The continuous curves are the calculated values of $\langle n_p \rangle$ and $\langle n_{\pi^\pm} \rangle$; the chain, dotted, and broken curves are the calculated values of $\langle n_{\pi^+} \rangle$, $\langle n_{\pi^0} \rangle$, $\langle n_{\pi^-} \rangle$; the open circles, black circles, black triangles, crosses, and open triangles are the corresponding experimental data from Refs. 11–34.

TABLE III. Integral characteristics of secondary protons in inelastic pp interactions (c.m.s.).

T, GeV	$\langle p_{\perp p}\rangle$, GeV/$c$	$\langle \mathscr{T}_p\rangle$, GeV	$\langle K_p\rangle$
10	0,38	0.62	0,34
20	0.39	0,99	0.31
10^2	0.41	3.17	0,30
$5\cdot10^2$	0.42	7,02	0.29
10^3	0.44	9,6	0,29
$1{,}5\cdot10^3$	0,44	11,4	0,29
$5\cdot10^3$	0.45	21.9	0,29

what more rapidly than s (i.e., is somewhat greater than $\mathscr{T}^{1/2}$). The values of $\langle K_p\rangle$ remain practically constant in the complete range of energies $T\gtrsim 20$ GeV. The mean kinetic energy $\langle \mathscr{T}_n\rangle$ of a neutron produced in a pp collision is 1.5–2 times less than $\langle \mathscr{T}_p\rangle$. With increasing energy of the primary particle,the energy $\langle \mathscr{T}_n\rangle$ increases somewhat more slowly than $\langle \mathscr{T}_p\rangle$; at $T=10$ GeV, $\langle \mathscr{T}_p\rangle/\langle \mathscr{T}_n\rangle = 1.4$, while at $T=10^2$ and 10^3 GeV this ratio is 2 and 2.5, respectively.

If the relative probability of proton and neutron production is taken into account, the mean energy carried away by a proton in an inelastic pp collision event is found to be approximately four times greater than the value for a neutron. At the same time, the inelasticity coefficient of the pp interaction, i.e., the fraction of energy carried away by all the newly produced particles,

$$\langle K\rangle = 1 - s^{-1/2}\langle n_p\rangle\{\langle \mathscr{T}_p\rangle + M_p\} - s^{-1/2}\langle n_n\rangle\{\langle \mathscr{T}_n\rangle + M_n\}, \tag{13}$$

is about 42%, in good agreement with known experimental data (see Fig. 8; for pn interactions, a similar value is obtained).[7)]

The fraction of energy carried away by a nucleon, $W(K_N, s)$, can be obtained by simple transformation:

$$\int \frac{d^2\sigma(x, p_\perp, s)}{dx\, dp_\perp^2}\, dx\, dp_\perp^2 = \int \frac{d^2\sigma_k(K_N, p_\perp, s)}{dK_N\, dp_\perp^2}\, dK_N\, dp_\perp^2 = \int W(K_N, s)\, dK_N.$$

The inelasticity coefficient of the NN interaction depends on the energies of the two nucleons at once [see Eq. (13)]. The distribution of this quantity, and also the distributions of K_{N_1} and K_{N_2} in the laboratory system, can be calculated by

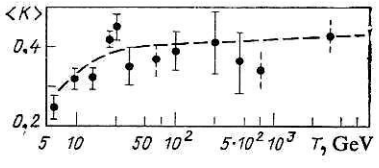

FIG. 8. Dependence of the inelasticity coefficient $\langle K\rangle$ in pN collisions on the energy of the primary proton. The broken curve is the calculation, and the experimental points are taken from Refs. 37–40.

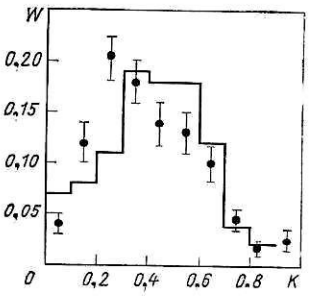

FIG. 9. Distribution of the inelasticity coefficient in pp collisions. The histogram represents the calculation for $T=10^2$–10^3 GeV; the points are the experimental data[41–43] for pN collisions obtained in the interval $T=20$–5×10^4 GeV.

the Monte Carlo method (by the method of statistical rejection; see Sec. 6) by specifying the values of the variables x and $p_\perp$ in accordance with (6) and calculating the corresponding nucleon energies $\mathscr{T}_{Ni} = (sx_i^2/4 + p_{\perp i}^2 + M_N^2)^{1/2} - M_N$, $i=1, 2$, in the laboratory of center-of-mass systems. This method of calculation is very effective.

In Fig. 9 we compare the distribution obtained in this manner with the experimental distribution for the range of energies $T\sim10^2$–10^3 Gev. It can be seen that the distributions are quite similar. However, the experimental points were obtained at different energies T and contain large errors, and the theoretical distribution $W(K)$ could therefore be preferable.

It should also be noted that although the mean value $\langle K\rangle$ depends weakly on the energy of the primary particles, the distributions $W(K)$ become broader with increasing T (Fig. 10).

By virtue of the symmetry of the NN system, the distribution $W(K)$ and the mean inelasticity coefficient $\langle K\rangle$ do not depend on whether they are considered in the center-of-mass or laboratory systems; at the same time, the nucleon coefficients $\langle K_{N_1}\rangle$ and $\langle K_{N_2}\rangle$, which are equal in the center-of-

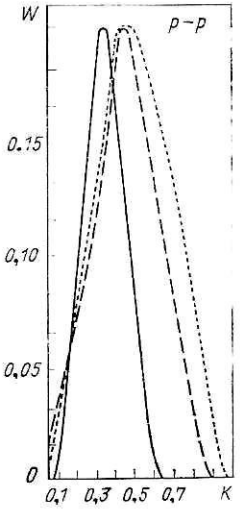

FIG. 10. Energy dependence of the inelasticity coefficient of pp interactions. The continuous, broken, and dotted curves are the results of calculation for $T=10$, 10^2, and 10^3 GeV, respectively.

[7)]In accordance with what is usually done in experiments, all secondary particles except for two nucleons are regarded as new. If a neutron is included among the new particles, then the corresponding inelasticity coefficient is $\langle K\rangle = 1 - \langle n_p\rangle\langle K_p\rangle = 0.55$ at $T=10$ GeV and 0.6 at $T\gtrsim 500$ GeV.

TABLE IV. Fraction of energy carried away by the leading proton and recoil proton in the *pp* interaction in the laboratory system.

T, GeV	$\langle K_{\text{lead}} \rangle$	$\langle K_{\text{rec}} \rangle$
10	0.53	0.131
10^2	0.55	0.019
10^3	0.56	0.0035

mass system, differ appreciably in the laboratory system (Table IV). The fraction of energy carried away by a leading nucleon remains practically constant for all $T \gtrsim 5$ GeV.

3. THE REACTION $N + N \to \pi + \ldots$

The inclusive cross section $Ed^3\sigma(x, p_\perp, s)/dp^3$ [in mb/GeV^2/c^{-3})] is in this case described by the expression (4). The values of the coefficients with which this expression gives the best description of the experimental data for *pp* and *pn* interactions at $T \gtrsim 5$ GeV are given in Table V. The corresponding values for *nn* collisions can be obtained by using charge-symmetry arguments (in Table V, it is necessary to interchange the positions of the π^+ and π^- mesons). The coefficients describing pion production are practically independent of the signs of the charge of the colliding nucleons to within the errors of the known experimental data.

It can be seen from Figs. 11–13 that the accuracy of the approximation is fairly good. Qualitatively, the dependence of the pion-production cross sections on x and $p_\perp$ is the same as for nonconserved nucleons, though the decrease in the pion cross sections at $|x| \sim 1$ takes place much more rapidly.

In Fig. 7, the mean multiplicities of the produced pions calculated by means of the expression (4) are compared with the experimental results. The calculated and experimental values agree well. In accordance with the experiments, the mean π^+ and π^0 multiplicities hardly differ, but significantly more π^- are produced. The difference $\langle n_{\pi^+} \rangle - \langle n_{\pi^-} \rangle$ remains practically constant (of order 0.5) in a wide range of energies from $T \gtrsim 10$ GeV to $T \sim 10^3$ GeV. The number of produced π^0 is 50–60% of the number of charged pions (Table VI). This agrees with the averaged experimental data of Refs. 22 and 29 but is somewhat higher than the values obtained in earlier measurements[46,47] (the difference is less than 20%). The relatively large π^0 fraction can be explained by the appreciable contribution of decaying resonance states.

To within the error of the approximation (4), the mean transverse momenta of the pions do not depend on the sign of the charge. Their magnitude is approximately a third smaller than the proton transverse momenta $\langle p_{\perp p} \rangle$ and increases very slowly with increasing primary energy T (Table VII). the approximating expressions reproduce well the $p_\perp - x$ correlation—the so-called sea-gull effect (Fig. 14):

$$\langle p_\perp(x) \rangle_E = \int_0^{p_{\perp\max}^2(x)} p_\perp E \frac{d^3\sigma}{dp^3} dp_\perp^2 \Big/ \int_0^{p_{\perp\max}^2(x)} E \frac{d^3\sigma}{dp^3} dp_\perp^2. \quad (14)$$

Figure 15 shows the calculated and the few currently known experimental values of the mean kinetic energy of the pions. Compared with the mean energy of the secondary protons, $\langle \mathcal{T}_\pi \rangle$ depends much more weakly on the energy of the primary particle—as $\mathcal{T}^\alpha$, where $\alpha \simeq 0.3$. This conclusion does not contradict the results of direct measurements of $\langle \mathcal{T}_\pi \rangle$, though the experimental information is as yet very sparse. In the complete region $\mathcal{T} \gtrsim 5$ GeV, $\langle \mathcal{T}_{\pi^+} \rangle > \langle \mathcal{T}_{\pi^-} \rangle$. The energy of the π^0 satisfies $\langle \mathcal{T}_{\pi^0} \rangle \simeq \langle \mathcal{T}_{\pi^+} \rangle$.

With regard to the fraction of energy carried away by the pions

where $\langle \mathcal{T}_\pi \rangle$ is determined by the relation (11) with M_p replaced by M_π, its value is about the same for π^+ and π^-. This agrees with the known experimental data (Table VIII). The energies expended on the production of the neutral and charged pions differ by a factor of about 2.

TABLE V. Values of the coefficients for approximating the inclusive cross sections of pions in *NN* collisions.

Coefficient	$pp \to \pi^+ \ldots$	$pp \to \pi^- \ldots$	$NN \to \pi^0 \ldots$	$pn \to \pi^+ \ldots$	$pn \to \pi^- \ldots$
a, mb/GeV^2	23	8	38	23	8
b	3	4	4	3 (6) *	6.5 (6) *
c	0.04	0.15	0	0.04	0.15
d	2	3.5	0.9	3	10
f	0.06	0.12	0.09	0.02	0
g	1.6	1.3	0.2	0.07	−2.4
h	11	11	11	11	11

*For the region $x < 0$.

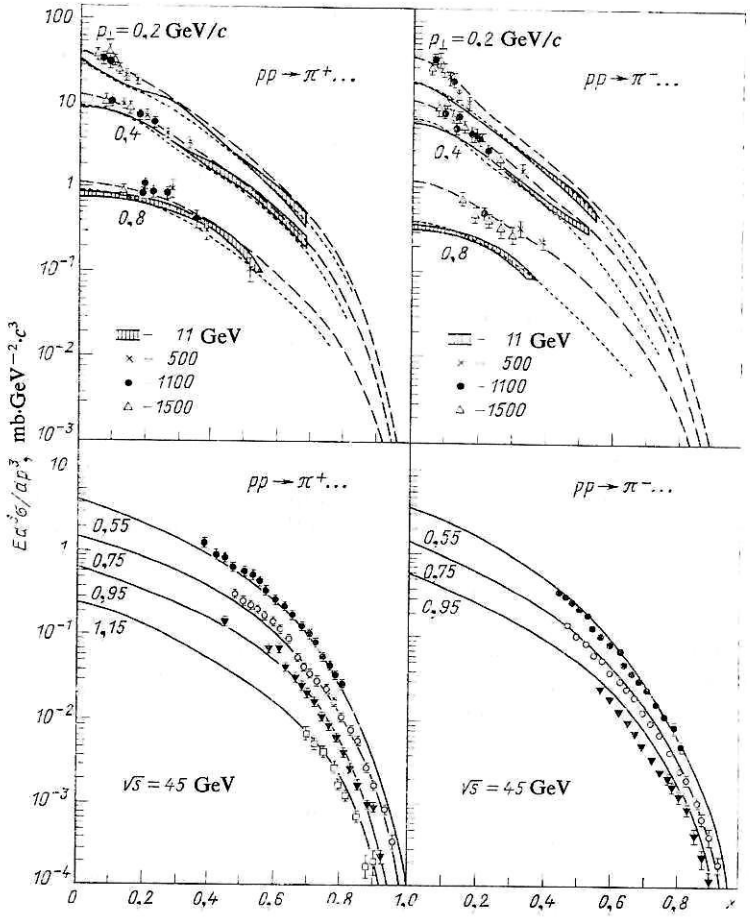

FIG. 11. Differential distributions of charged pions in pp collisions. The dotted and broken curves are the calculations for $T = 10$ and 10^3 GeV, respectively. The experimental data are taken from Ref. 7.

4. THE REACTIONS $\pi + N \to \pi + \ldots$ AND $\pi + N \to N + \ldots$

A feature of these reactions is that here there is not the pronounced difference between the properties of the conserved and nonconserved particles observed in the case of NN interactions. This is due to the fact that pions are produced in both central and fragmentation processes.

We shall describe the distributions of the conserved particles (pion with $x > 0$ and a nucleon emitted in the opposite hemisphere with $x < 0$) by means of an expression that apart from the numerical values of the coefficients is the

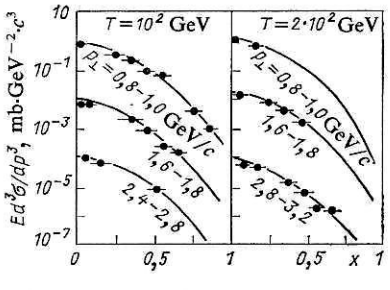

FIG. 12. Differential distribution of π^0 mesons in pp collisions. The curves represent the calculations; the points are from the experiment of Ref. 44.

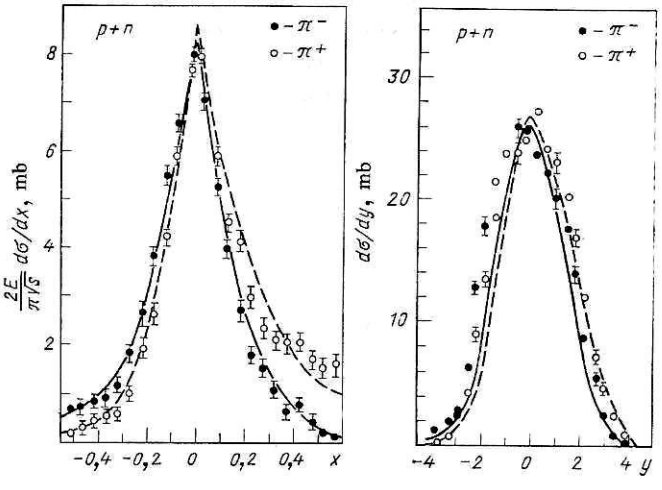

FIG. 13. Integrated cross sections $(2E/\pi\sqrt{s})(d\sigma/dx)$ and $(d\sigma/dy)$, of the reaction $p + n \to \pi^\pm + \ldots$; $y = 0.5 \ln [(E + p_\parallel)/(E - p_\parallel)]$. The primary energy is $T = 194$ GeV. The points are the experimental data from Ref. 45; the continuous and broken curves are the calculations for π^- and π^+, respectively.

TABLE VI. Ratio of the mean multiplicities of neutral and charged pions in elastic pp interactions.

T, GeV	$\langle n_{\pi^0}\rangle/\langle n_{\pi^+}\rangle$	
	Theory	Experiment*
10	0,58	0,57±0.04
20	0,57	0,59±0.04
100	0,55	0.58±0.04
500	0,53	0,57±0.05
10^3	0.52	0.56±0,08
$1,5\cdot10^3$	0,51	0,55±0.08

*The experimental values are taken from the curves $\langle n(T)\rangle$ that approximate the results of the measurements in Refs. 22 and 29.

same as the corresponding expression (6) for NN collisions. The values of the coefficients are given in Tables IX and X.

In πN collisions, the nonconserved particles include not only particles having a charge different from the charges of the colliding particles but also a nucleon or meson that keep the same charge but are emitted in the hemispheres opposite to the directions of motion of the corresponding primary particles (for example, in the case of the π^-p interaction such is a proton with $x>0$ and a π^- meson with $x<0$). As in the case of NN interaction, we again choose the inclusive spectrum of the nonconserved particles, mesons and nucleons, in the form (4) with coefficients from Table XI. These coefficients apply both for $x>0$ and for $x<0$. The only exception is the coefficient b, whose values for $x<0$ are given in brackets.

The examples given in Figs. 16–19 indicate the quality of the expressions (4) and (6) as approximations of the experimental data on πN interactions.

In Fig. 20 and Table XII we give data on the mean multiplicities $\langle n_c\rangle$ of the secondary particles; the integration of the spectra of the conserved and nonconserved particles is over the corresponding values of x (forward and backward hemispheres of particle emission). The calculated curves are close to the experimental points, though for $T\gtrsim 100$ GeV the experimental values of $\langle n_{\rm ch}\rangle$ lie systematically somewhat above the calculated curve. This is due to the fact that the experimentally measured total multiplicity of all the charged particles exceeds the calculated values of

TABLE VII. Values of $\langle p_{\perp\pi}\rangle$ in pp collisions.

T, GeV	$\langle p_{\perp\pi^-}\rangle$, MeV/$c$	
	Theory	Experiment*
10	306	307±6
20	317	310±4
10^2	323	340±10
10^3	332	340±30
$4,1\cdot10^3$	340	270±30

*See Refs. 39, 40, and 49.

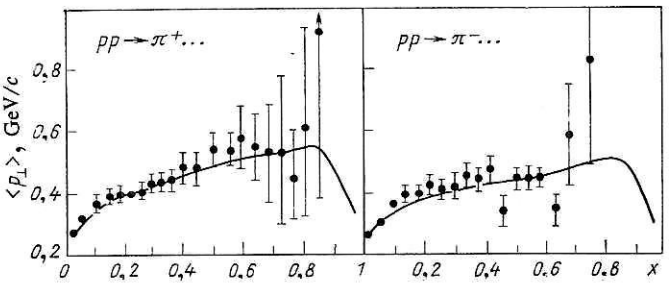

FIG. 14. Mean transverse momentum of the π^+ and π^- mesons in the inclusive pp reaction at energy $T=68$ GeV. The curves are the result of calculation; the points correspond to the experiment of Ref. 51.

$\langle n^*_{\rm ch}\rangle = \langle n_p\rangle + \langle n_{\pi^\pm}\rangle$ by the multiplicity $\langle n_{s,\bar p}\rangle$ of the strange particles and antiprotons. The difference $\langle n_{\rm ch}\rangle_{\rm exp} - \langle n_{\rm ch}\rangle_{\rm th}$ agrees with the experimental multiplicity $\langle n_{s,\bar p}\rangle$.

As in pp interactions (see Sec. 3), the largest multiplicity is that of the particles that do not change the sign of the charge. The pion multiplicity becomes independent of the charge only at very high energies $T\gtrsim 10^3$ GeV. At the same time, the fraction of produced π^0 in the complete range of energies $T\gg 1$ GeV remains almost constant: $\langle n_{\pi^0}\rangle/\langle n_{\pi^\pm}\rangle \simeq 40$–$50\%$.

The mean transverse momenta of the conserved particles, nucleons and pions, are appreciably greater than the practically equal transverse momenta of the remaining particles (see Table XIII, in which the π^-p interaction is considered as an example). The energy dependence of $\langle p_\perp\rangle$ is very weak.

As in the case of NN interactions considered above, the approximating expression reproduces well the $p_{\perp x}$ correlations (Fig. 21).

The distinguished nature of the conserved particles is also manifested in their energy, which, especially for a nucleon, appreciably exceeds the energy of the remaining particles. For example, in the case of π^-p collisions the mean proton energy in the center-of-mass system satisfies $\langle \mathcal{T}_p\rangle \gtrsim \mathcal{T}^{1/2}$, as in pp collisions. At the same time, the pion energy is $\sim\mathcal{T}^\alpha$, where $\alpha=0.3$; further, $\langle \mathcal{T}_{\pi^+}\rangle \simeq \langle \mathcal{T}_{\pi^0}\rangle$,

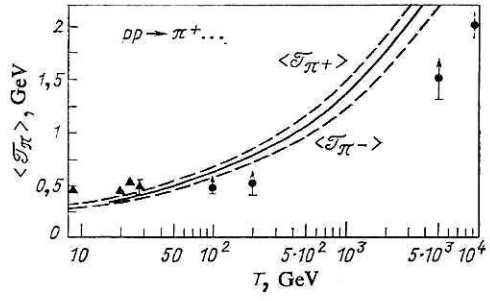

FIG. 15. Mean kinetic energy of the mesons in pp collisions (c.m.s.). The continuous curve is the calculation for $\pi^\pm$ mesons; the upper and lower broken curves are for π^+ and π^-, respectively. The black triangles are the experimental data for pp interactions; the black circles are the experimental data for the interaction of protons with light nuclei.[39,48]

TABLE VIII. Fraction of energy $\langle K_\pi \rangle$ carried away by π^- and π^0 mesons in pp collisions (c.m.s.).

$\langle K_{\pi^-} \rangle$			$\langle K_{\pi^0} \rangle$		
T, GeV	Theory	Experiment*	T, GeV	Theory	Experiment*
9	0.07	0.13±0.03	9	0.12	0.15±0.02 **
18	0.08	0.11±0.06	20	0.13	0.16±0.02 **
68	0.09	—	68	0.14	0.12±0.01
205	0.10	—	205	0.15	0.14±0.02
250	0.11	0.12±0.04	300	0.16	0.17±0.03
10^3	0.13	0.11±0.08	10^3	0.17	0.17±0.01

*See the compilations of Refs. 39 and 50.
**For $p + {}^{12}C$ interactions.

TABLE IX. Values of the coefficients for calculation of the spectra of conserved pions and nucleons in the region $|x| < 0.7$.

	Reaction	a, mb/GeV^2	b	c	d	f, (GeV/c)$^{-2}$	g	μ^2, (GeV/c)^2	u, mb/GeV^2	v
$\pi - p$	$\pi^- p \to \pi_{con}$ ...	103	27	−0.4	6.3	0.26	−3.1	1.27	0.05	0.7
	$\pi^+ p \to p$...	2.1	−0.4	0.04	6.2	0.1	5.5	1.20	2.1	−0.35
$\pi - n$	$\pi^- n \to \pi_{con}$ ...	80	15	−0.6	6.4	0.3	−2.4	1.26	5	0.04
	$\pi^+ n \to p$ ...	2.1	−0.16	0.04	6.2	0.1	4.7	1.26	1.3	−0.25

TABLE X. Values of the coefficients for calculation of the spectra of conserved pions and nucleons in the region $|x| \geqslant 0.7$.

Coefficients that are the same for all reactions				$\pi p \to p$...		$\pi n \to p$...		$\pi p \to \pi_{con}$ ...		$\pi n \to \pi_{con}$ ...	
G, mb/GeV^2				15		20		—		—	
R, (GeV/c)$^{-2}$				0.02		0.01		—		—	
γ, (GeV/c)$^{-2}$				0.8		0.9		—		—	
i	α_i	β_i	γ_i, (GeV/c)$^{-2}$	G_i, mb/GeV^2	R_i, (GeV/c)$^{-2}$	G_i, mb/GeV^2	R_i, (GeV/c)$^{-2}$	G_i, mb/GeV^2	R_i, (GeV/c)$^{-2}$	G_i, mb/GeV^2	R_i, (GeV/c)$^{-2}$
1	0	0	1.5	32	1.1	4.1	3.0	3.5	2.8	5.5	1.7
2	−0.5	−0.5	1.5	36	5.3	—	—	32	19	6.5	4.6
3	0	−1.0	0.2	—	—	—	—	0.37	2.1	0.08	1.2
4	0	−0.5	0.85	—	—	—	—	0.05	0.18	—	—

TABLE XI. Values of the coefficients for the spectrum of nonconserved particles.

Coefficient	$\pi^0 p \to \pi^{\mp} \pi^{\pm}$...	$\pi^0 n \to \pi^{\mp} \pi^{\pm}$...	$\pi N \to \pi^0$...	$\pi p \to \pi_{con}$ ...*	$\pi n \to \pi_{con}$ ...*	$\pi N \to N$...**
a, mb/GeV^2	20	20	22	29	20	2
b	2 (2.1)*	2 (4)*	1.7 (2)*	2.6	5	3
c	0.02	0.02	0.01	0.02	0.02	−0.01
d	2	1.8	1.4	0.93	1.3	1.0
f	0.01	0.01	0.04	0.01	0.01	−0.1
g	0.6	0.7	0.55	1.8	1.1	−2.05
h	11	11	11	6	6	3

*For the region $x < 0$.
**For the region $x > 0$.

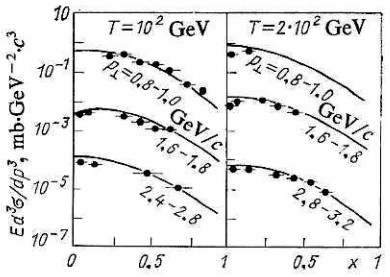

FIG. 16. Differential distributions of charged particles in inelastic πp collisions. The points are calculated for $T = 16$ GeV; the experimental curves are taken from Refs. 52 and 53. The corresponding values of $p_\perp$, in GeV/c, are given next to the curves.

and the energy of the π^- mesons, among which there are fast leading particles besides the conserved particles, is approximately 1.5 times greater (Fig. 22).

At a given primary energy T, the kinetic energy of the secondary pions in πN collisions is on the average 10–20% greater than in the case of NN interactions (in the center-of-mass system).

The inelasticity coefficient $\langle K \rangle$, which characterizes the expenditure of energy on the production of new particles, is determined much less definitely in the case of πN collisions than for NN collisions. In accordance with its physical

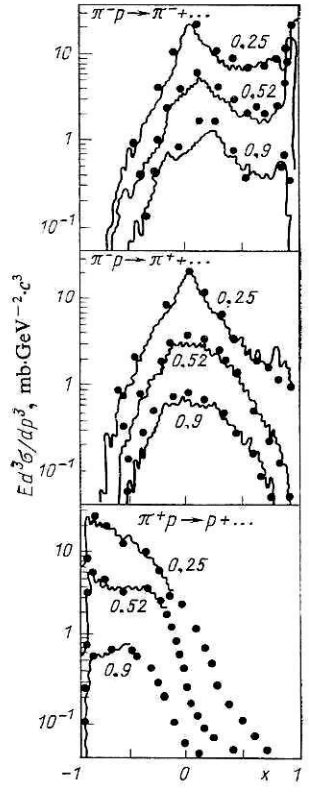

FIG. 17. Differential distributions of π^0 mesons produced in $\pi^- p$ collisions at energy T. The curves represent the calculations, and the experimental points are taken from Ref. 44. The values of $p_\perp$, in GeV/c, are given next to the curves.

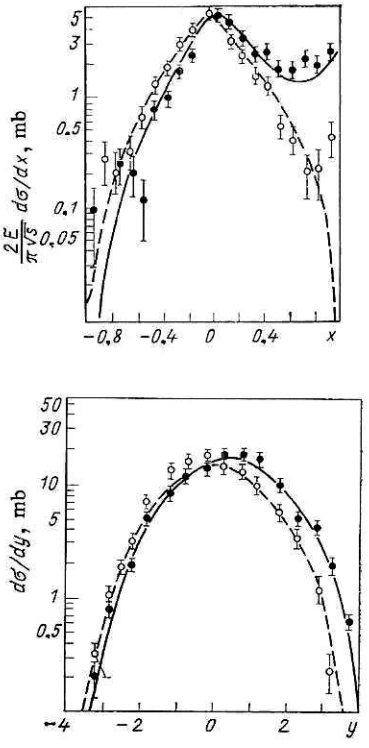

FIG. 18. Distributions of $\pi^\pm$ mesons produced in $\pi^- p$ collisions at $T = 40$ GeV with respect to the variable x and the rapidity y (cf. Fig. 13). The continuous curves are the calculated π^- distributions; the broken curves are the calculation for π^+; the points are from the experiment of Ref. 54.

meaning, the coefficient $\langle K \rangle$ should be defined as

$$\langle K \rangle = 1 - s^{-1/2} \{ \langle \mathcal{T}_N \rangle + \langle \mathcal{T}_{\pi_{\text{lead}}} \rangle + M_N + M_\pi \}, \qquad (15)$$

where $\langle \mathcal{T}_N \rangle$ and $\langle \mathcal{T}_{\pi_{\text{lead}}} \rangle$ are the mean kinetic energies of the secondary nucleon and the leading pion, and M_N and M_π are their masses. However, at the present time there are no generally accepted criteria for distinguishing the leading

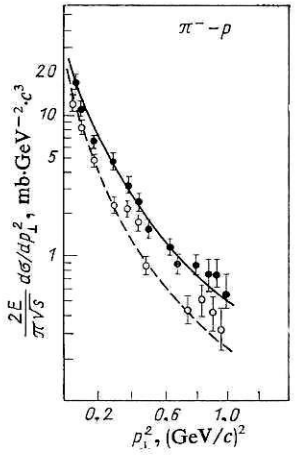

FIG. 19. Integrated cross sections of $\pi^\pm$ production in $\pi^- p$ collisions at $T = 40$ GeV. The continuous and broken curves are for π^- and π^+, respectively; the points are taken from the experiment of Ref. 54.

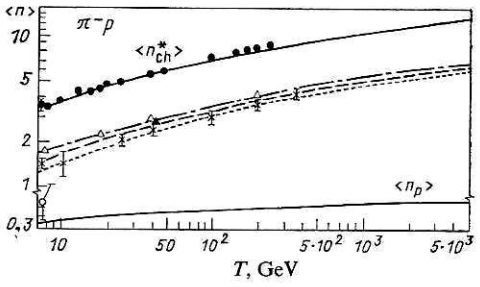

FIG. 20. Mean multiplicity of particles produced in inelastic $\pi^- p$ interactions. The continuous curves are the calculated values of $\langle n_p \rangle$ and $\langle n_{ch}^* \rangle$; the chain, dotted, and broken curves are the calculated values of $\langle n_{\pi^-} \rangle$, $\langle n_{\pi^0} \rangle$, and $\langle n_{\pi^+} \rangle$; the open circles, black circles, open triangles, black triangles, and crosses are the experimental multiplicities $\langle n_p \rangle$, $\langle n_{ch}^* \rangle$, $\langle n_{\pi^-} \rangle$, $\langle n_{\pi^+} \rangle$, and $\langle n_{\pi^0} \rangle$ (Refs. 22, 33, and 55–69).

TABLE XII. Relative multiplicity of neutral and charged pions in inelastic $\pi^- p$ interactions (the references are given in square brackets).

T, GeV	$\langle n_{\pi^0} \rangle / \langle n_{\pi^\pm} \rangle$	
	Theory	Experiment
7	0,41	0.40±0,12 [44, 55, 56]
10	0,44	—
25	0,46	0,47±0,05 [58]
40	0,46	0,45±0,01 [59]
100	0,47	0,46±0.06 [33] *
205	0,48	0.56±0.09 [67] *
10^3	0,49	—

*Using the value $\langle n_{\pi^\pm} \rangle = \langle n_{ch} \rangle_{exp} - \langle n_p \rangle_{th}$.

particle among the other conserved particles, and the relation (15) is often replaced by

$$\langle K \rangle = \langle \Delta E_\pi \rangle \, s^{-1/2}, \tag{16}$$

where ΔE_π is the total energy of all the secondary pions in the center-of-mass system after subtraction of the mean energy $\langle E_{\pi^\pm} \rangle = \langle \mathscr{T}_{\pi^\pm} \rangle + M_{\pi^\pm}$ of one secondary pion. The values of $\langle K \rangle$ calculated in this manner for the case of $\pi^- p$ collisions are given together with the known experimental data in Table XIV.

The value of $\langle K \rangle$ determined in accordance with (15) is almost twice the inelasticity coefficient of NN interactions (cf. Fig. 8) and increases with increasing energy T of the primary particle. This is due to the large contribution of the leading pion.

The situation is simpler with regard to the partial inelasticity coefficients $\langle K_c \rangle$ for a secondary nucleon and pions with charge different from that of the primary pion [cf. Eq. (14)]. The uncertainty in these coefficients is due solely to the choice of the coordinate system. As in the case of NN interactions, the proton inelasticity coefficient $\langle K_p \rangle$ hardly depends on the energy T, while the pion inelasticity coefficients increase very slowly with increasing T (see Tables XIV and XV). At all energies $T \gtrsim 10$ GeV, the ratio of the inelasticity coefficients of the nonconserved pions of different signs of the charge (for example, $\langle K_{\pi^0} \rangle / \langle K_{\pi^+} \rangle$ in the case of $\pi^- p$ collisions) is equal to unity with an error of a few percent.

5. PROPERTIES OF THE LEADING PARTICLES

In inelastic interactions of high-energy hadrons, the main fraction of the energy of the colliding particles is, as a rule, carried away by just a few (in the laboratory system, usually one) particles having energies that are sharply distinguished; these are the so-called leading particles. Numerous studies have been made of the properties and conditions of production of these particles (see, for example, Refs. 81–86, in which the corresponding bibliography can be found). Unfortunately, the experimental data are to a considerable degree scattered and patchy; many were obtained by analyzing hadron–nucleus interactions with very crude allowance for intranuclear interactions. In addition, different authors use different definitions of a leading particle. However, what is known already indicates a specific mechanism of production of this component.

The approximations of the inclusive cross sections considered above represent a large body of the experimental information on the particle spectra at both low and very high energies $\mathscr{T}$, and they can be used for systematic study of the properties of the high-energy component of the secondary

TABLE XIII. Mean transverse momentum of secondary particles in inelastic πp interactions (the references are given in square brackets).

T, GeV	$\langle p_{\perp p} \rangle$, GeV/c	$\langle p_{\perp \pi^-} \rangle$, GeV/c	$\langle p_{\perp \pi^+, \pi^0} \rangle$, GeV/c
10	0,42	0,36	0,30
	(0,42±0,03) * [70, 71]	—	(0,30±0,02) [70, 71]
20	0,43	0,37	0,32
	(0,42±0,04) [22]	(0,37±0,01) [54, 73]	—
40	0,43	0,38	0,33
	—	(0,356±0,004) [54]	(0,368±0,004) [54]
10^2	0,44	0,39	0,34
10^3	0,45	0,40	0,35
$5 \cdot 10^3$	0.46	0,42	0,36

*The experimental data are given in brackets.

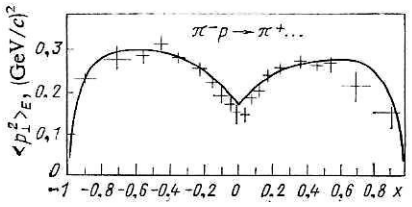

FIG. 21. Correlations of the values of $\langle p_\perp^2(x)\rangle_E$ and x for π^+ mesons in the inclusive $\pi^- p$ reaction at $T = 15$ GeV. The curve represents the calculation; the points are from the experiment of Ref. 80.

particles of different species, including comparison of different ways of characterizing quantitatively the leading-particle effect.

In Table XVI and in Figs. 23 and 24 we show how many particles in inelastic pp and $\pi^- p$ collisions are produced with kinetic energy greater than $\mathscr{T}$:

$$\langle n(\mathscr{T}, s)\rangle = \{\sigma_+[1, \mathscr{T}, s] + \sigma_-[1, \mathscr{T}, s]\}/\sigma_{1n}, \qquad (17)$$

which contains the functionals

$$\sigma_+[z, \mathscr{T}, s] = \int_{x(\mathscr{T})}^{x(\mathscr{T}_{max})} \varphi_+[z, x, s]\, dx, \quad \sigma_-[z, \mathscr{T}, s]$$

$$= \int_{-x(\mathscr{T}_{max})}^{-x(\mathscr{T})} \varphi_-[z, x, s]\, dx, \quad \varphi_\pm[z, x, s] =$$

$$= \frac{\pi\sqrt{s}}{2} \int_0^{p_\perp^2(x, \mathscr{T})} \left(E\frac{d^3\sigma(x, p_\perp^2, s)}{dp^3}\right)_\pm \frac{z(\pm|x|, p_\perp^2, s)\, dp_\perp^2}{(x^2 s/4 + p_\perp^2 + M_c^2)^{1/2}},$$

$$x(\mathscr{T}) = 2\sqrt{\mathscr{T}(\mathscr{T} + 2M_c)/s}, \qquad (18)$$

$$\mathscr{T}_{max} = (s + M_c^2 - M_x^2)/(2s^{1/2}) - M_c.$$

The indices + and − indicate that the choice of the expressions for the inclusive cross sections must correspond to the forward ($x > 0$) and backward ($x < 0$) hemispheres relative to the direction of motion of the incident particle. In the figures, the initial energy $T = 100$ GeV is considered as an example.

It can be seen from the table that the number of high-energy particles is almost independent of the primary energy T and changes little on the transition from one reaction to another. At the same time, as can be seen from the figures, the particles clearly distinguished by their energy are in the majority of cases those that preserve the electric charge and baryon number of the primary particles; the production of high-energy particles differing in the sign of the charge from the primary particles is less probable. In the case of NN collisions, the probability of production of a leading meson is very small. In πN collisions, in which the primary mesons and nucleons are on an equal footing as regards the kinematic conditions, a nucleon is nevertheless more often distinguished in energy than a pion when $\mathscr{T} > 0.35\mathscr{T}_{max}$ (Table XVII).

In Figs. 23 and 24 and in Tables XVIII and XIX we give the values of the mean angle of emission of particles in the forward and backward hemispheres:

$$\langle\theta_\pm(\mathscr{T}, s)\rangle = \sigma_\pm\left[\tan^{-1}\left(\frac{p_\perp}{p_\parallel}\right), \mathscr{T}, s\right] \Big/ \sigma_\pm[1, \mathscr{T}, s]. \qquad (19)$$

In the case of pp collisions, $\langle\theta_+\rangle = \langle\theta_-\rangle$; in $\pi^- p$ collisions there are virtually no nucleons in the forward hemisphere,

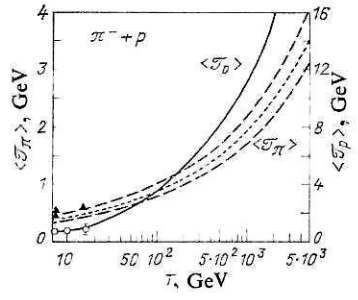

FIG. 22. Mean kinetic energy of the secondary particles in inelastic $\pi^- p$ interactions (c.m.s.). The continuous curve gives the energy of the protons; the upper and lower broken curves give $\langle \mathscr{T}_{\pi^-} \rangle$ and $\langle \mathscr{T}_{\pi^+} \rangle$, respectively; the dotted curve gives the mean energy of the charged pions; the black triangles are the averaged experimental data for the charged pions, and the open circles are the experimental data for the protons (Refs. 39, 72, and 74–76).

TABLE XIV. Inelasticity coefficients of $\pi - p$ interactions in the center-of-mass system.

T, GeV	$\langle K\rangle$ Theory	$\langle K\rangle$ Experiment (Ref. 39)	$\langle K_p\rangle$
7	0,47	0,49±0,08	0,30
10	0,48	0,57±0,05	0,30
16	0,51	0,56±0,06	0,30
10^2	0,59	—	0,29
10^3	0,67	—	0,26

TABLE XV. Relative fraction of energy expended in $\pi^- p$ interactions on π^0 production in the laboratory system (the references are given in square brackets).

T, GeV	Theory	Experiment
10,5	0,19	0,22±0,01 [77]
18,5	0,20	0,21±0,01 [78, 79]
40	0,23	0,25±0,01 [79]
10^2	0,24	—
10^3	0,26	—
$5\cdot10^3$	0,27	—

TABLE XVI. Mean number $\langle n\rangle = \langle n_N\rangle + \langle n_\pi\rangle$ of high energy particles in pp and $\pi^- p$ collisions at energy T.

Interaction	T, GeV	$\mathcal{T}/\mathcal{T}_{max}$ > 0.2	> 0.4	> 0.7
$p-p$	10	1.7	1.0	0.48
	10^2	1.9	1.0	0.48
	10^3	1.9	1.0	0.48
$\pi^- - p$	10	2.0	1.1	0.47
	10^2	2.3	1.1	0.51
	10^3	2.6	1.2	0.51

and therefore the angle $\langle\theta_+\rangle$ for nucleons is not given.

High-energy nucleons are produced predominantly in a narrow solid angle around the velocity vector of the primary proton. High-energy pions are also emitted in a narrow angle around the direction of motion of the primary particle. In the $\pi^- p$ reaction, such pions are emitted mainly in the direction of motion of the primary pion; only a small number of particles are emitted in the opposite direction (see Table XIX).[8] It can be seen from Figs. 23 and 24 that, as a rule, the mesons are emitted in an appreciably wider angle than the nucleons. The angles $\langle\theta\rangle$ of the high-energy particles depend weakly on the type of reaction and decrease with increasing primary energy. The radius of the spatial region with which the process of production of high-energy particles is associated is

$$\langle\rho(\mathcal{T}, s)\rangle = \hbar/\langle p_\perp(\mathcal{T}, s)\rangle = \\ = \hbar\sigma_{in}\langle n(\mathcal{T}, s)\rangle/\{\sigma_+[p_\perp, \mathcal{T}, s] + \sigma_-[p_\perp, \mathcal{T}, s]\}. \quad (20)$$

The production of particles occurs mainly in a region with $\rho \simeq (0.4\text{–}0.7)\times 10^{-13}$ cm; the nucleons are produced, on the average, at larger radii than the pions. The values of $\langle p\rangle$ are weakly sensitive to the energy T of the primary particles (Table XX).

The characteristic features of the "leading-particle effect" indicate that in a wide range of energies, up to the maximal $T \sim 10^3$ GeV at which there are still measurements of the energies of the produced particles, the high-energy nucleons are produced mainly in "glancing" peripheral collisions, while a comparatively small fraction of the total

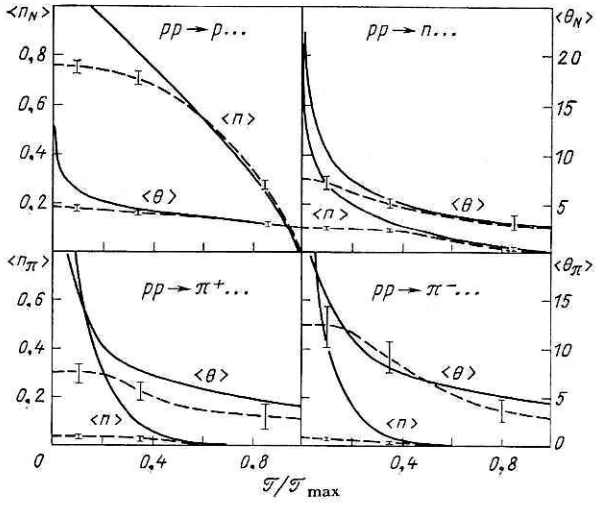

FIG. 23. Mean number of secondary particles $\langle n\rangle$ with energy greater than $\mathcal{T}$ and the mean emission angle $\langle\theta\rangle$ of these particles (in degrees). Inelastic pp interaction at $T = 100$ GeV. The broken curves are the corresponding distributions for the "fastest secondary particle" calculated by the Monte Carlo method. The statistical errors of the calculation are indicated.

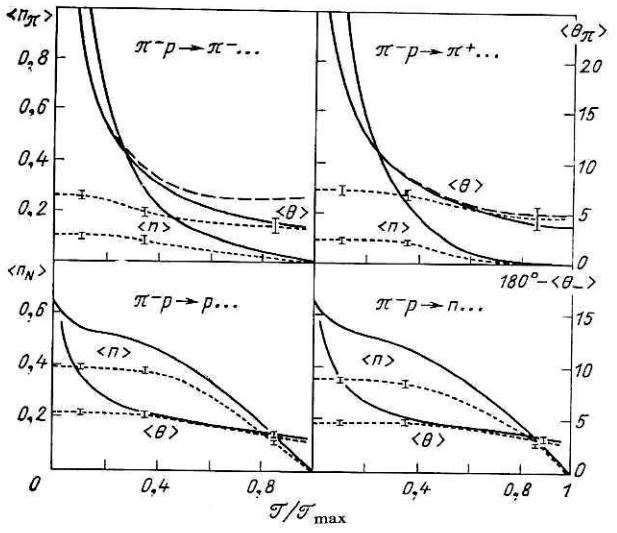

FIG. 24. The same as in Fig. 23. Inelastic $\pi^- p$ interaction at $T = 100$ GeV. The continuous curves represent $\langle\theta_+\rangle$, the broken curves $\langle\theta_-\rangle$; the dotted curves are the mean multiplicity and the mean emission angle $\langle\theta_+\rangle = \langle\theta_-\rangle$ of the "fastest secondary particle" calculated by the Monte Carlo method. The statistical errors of the calculations for these curves are indicated.

TABLE XVII. Ratio of the mean numbers of high-energy nucleons and pions $\langle n_N\rangle/\langle n_\pi\rangle$, in pp and $\pi^- p$ collisions at energy T.

Interaction	T, GeV	$\mathcal{T}/\mathcal{T}_{max}$ > 0.2	> 0.4	> 0.7
$p-p$	10	2.3	8	~ 100
	10^2	1.6	8	~ 100
	10^3	1.5	8	~ 100
$\pi^- - p$	10	0.61	1.6	4.2
	10^2	0.52	1.5	4.2
	10^3	0.43	1.4	4.2

[8] A small number of pions in the neighborhood of $\theta \sim \pi$ significantly increases the mean emission angle $\langle\theta\rangle = \{\langle\theta_+\rangle\sigma_+ + \langle\theta_-\rangle\sigma_-\}/\{\sigma_+ + \sigma_-\}$ of the pions. For example, at $T = 100$ GeV the angle $\langle\theta_-\rangle$ for leading pions with energies $\mathcal{T} > 0.7\mathcal{T}_{max}$ exceeds the angle $\langle\theta_+\rangle$ by almost an order of magnitude. Therefore, it is clearer to consider $\langle\theta_+\rangle$ and $\langle\theta_-\rangle$ separately.

TABLE XVIII. Mean emission angle $\langle\theta_p\rangle$ of high-energy protons in pp and $\pi^- p$ collisions at energy T (in degrees).

Interaction	T, GeV	$\mathcal{T}/\mathcal{T}_{max}$ > 0,2	> 0,4	> 0,7
$p-p$	10	15	11	10
	10^2	5,1	4,0	3.2
	10^3	2,0	1,5	1,1
$\pi^- - p$	10	16	14	11
	10^2	7	5,2	3.8
	10^3	4	1,7	1.3

TABLE XX. Mean radius $\langle\rho\rangle$ of the spatial region associated with production of nucleons and pions at energy $\mathcal{T} > 0.7\,\mathcal{T}_{max}$.

Interaction	T, GeV	$\langle\rho_N\rangle$, 10^{-13} cm	$\langle\rho_\pi\rangle$, 10^{-13} cm
$p-p$	10	0,65	0,51
	10^2	0,58	0,43
	10^3	0,55	0,41
$\pi^- - p$	10	0,52	0,53
	10^2	0,49	0,47
	10^3	0,48	0,44

energy $s^{1/2}$ goes over into the pion component, this fraction being smaller, the more peripheral is the collision. This is confirmed by all the currently available experimental data.

It can be clearly seen from the tables and figures that it is not possible to make a sharp distinction between the leading and remaining secondary particles. The limiting condition $T' > 0.7T$ frequently used in experimental studies, i.e., $\mathcal{T} > (0.6\text{–}0.8)\mathcal{T}_{max}$ is very arbitrary. Although the leading-particle effect becomes more pronounced on the transition to larger values of $\mathcal{T}/\mathcal{T}_{max}$, at $T = 100$ GeV particles with $\mathcal{T} > 0.2\ \mathcal{T}_{max}$ and at $T = 10^3$ GeV particles with $\mathcal{T} > 0.1\mathcal{T}_{max}$ can already be regarded as leading particles. For the overwhelming majority of such particles, the condition $\theta \sim 0$ or $\theta \sim \pi$, which is used by some authors as an additional criterion for distinguishing leading particles, is satisfied.

It was suggested in Ref. 84 that the particle with the greatest kinetic energy in a given inelastic interaction should be chosen as the leading secondary particle. Theoretically, such a choice of the leading particle can be simulated by using the Monte Carlo method, which makes it possible to find the characteristics of all secondary particles for each individual interaction event.

We now consider the results relating to the fastest secondary particle.

We note first that in the center-of-mass system, in which the production of a particle with high energy $\mathcal{T}$ and small emission angle $\theta \sim 0$ is usually accompanied by the production of a compensating very fast particle in the region $\theta \sim \pi$ by virtue of the momentum conservation law, the identification of the leading particle as the most energetic (fastest) one distinguishes only some of the high-energy particles: $\Delta_i(\mathcal{T}) \equiv n_i(\mathcal{T}) - n_i(\mathcal{T}_{max}) \geqslant 0$ $(i = p,\ n,\ \pi)$. The total difference of the multiplicities

$$\int_0^{\mathcal{T}_{max}} \{\Delta_p(\mathcal{T}) + \Delta_n(\mathcal{T}) + \Delta_\pi(\mathcal{T})\}\, d\mathcal{T} = \langle n\rangle - 1$$

may be very appreciable. However, for $\mathcal{T} > 0.5\ \mathcal{T}_{max}$ the difference is small and is entirely determined by the contribution of the pions; for the nucleons, $n(\mathcal{T}) \simeq n(\mathcal{T}_{max})$ (see Figs. 23 and 24 and Table XXI).

As a rule (even in the case of πN collisions), a nucleon is the most energetic secondary particle. The probability that a pion has the distinguished energy is much less; in the region $\mathcal{T} \gtrsim 0.5\mathcal{T}_{max}$ it is very small.

Like the mean multiplicity, the angular distributions of the fastest and of all the high-energy nucleons are practically identical for $\mathcal{T} > 0.5\mathcal{T}_{max}$. These distributions are also nearly the same for the pions. At the same time, in NN collisions, for which the multiplicity of the fastest pions is somewhat less than the total multiplicity of the high-energy pions even at large $\mathcal{T}$ (Fig. 24), the emission angles of the high-

TABLE XIX. Ratio $\sigma_+[1, \mathcal{T}, s]/\sigma_-[1, \mathcal{T}, s]$ of the number of high-energy pions in $\pi^- p$ interactions emitted in the forward and backward hemispheres.

T, GeV	$\mathcal{T}/\mathcal{T}_{max}$ > 0,2	> 0,4	> 0,7
10	1,6	2,2	5,8
10^2	1,6	2,1	6,8
10^3	1,6	2,1	9,3

TABLE XXI. Probability that the fastest secondary particle is a proton, neutron, or pion (%). The primary energy is $T = 100$ GeV.

Particle	Interaction $p-p$	$\pi^- - p$
p	75±2,5	39±1,5
n	11±1	34±1,5
π^-	3±0.5	11±0,5
All π	14±1	27±1
$(p+n)/\pi$	6,1±0,6	2,7±0,1

energy pions have a wider range. This is due to the contribution of channels with the production of several high-energy particles at once.

Thus, at high energies the identification of leading particles on the basis of the absolute and relative values of $\mathscr{T}$ leads to the same result. At lower energies, comparison of the two methods of selection gives interesting additional information, though it is true that the experimental investigation of this question requires higher statistics of the detected events.

6. SIMULATION OF INDIVIDUAL INELASTIC INTERACTION EVENTS

The method proposed in Refs. 1 and 2 for calculating the characteristics of the particles produced in inelastic πN or NN collisions is based on Monte Carlo determination of the angles and energies of these particles from the factorized inclusive distribution $d^3\sigma(\theta, \mathscr{T}, s)/dp^3 = f(\cos\theta, s)*\varphi(\mathscr{T}, s)$.

A similar method can also be used for the two-dimensional inclusive distributions $Ed^3\sigma(x, p_\perp, s)/dp^3$. However, in this case the correlations between x, $p_\perp$, and the electric charge Q must be taken into account for each individual secondary particle.

Figures 25 and 26 illustrate one of the possible ways of determining the particle characteristics. The calculation begins with the statistical sampling of the sign of the electric charge of the particle, Then from the equation

$$\int_{-x_{\max}}^{x'} W(x, 0, s)\, dx = \xi_1, \tag{21}$$

where

$$W(x, p_\perp, s) = E\frac{d^3\sigma(x, p_\perp, s)}{dp^3}\Big/\int_{-x_{\max}}^{+x_{\max}} E\frac{d^3\sigma(x, p_\perp, s)}{dp^3}dx,$$

and ξ_1 is a random number distributed uniformly in the interval [0, 1], the value of the variable x is found.[9] The next step is to choose two random numbers ξ_2 and ξ_3 uniformly distributed in the intervals $0 \leqslant \xi_2 \leqslant p^2_{\perp\max}$ and $0 \leqslant \xi_3 \leqslant W(x, 0, s)$ and to use the Neumann rejection method to determine $p_\perp$ from the distribution $W(x, p_\perp, s)$. Additional correlations are

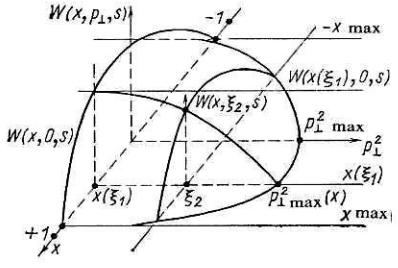

FIG. 25. The function $W(x, p_\perp, s)$ for a given value of s

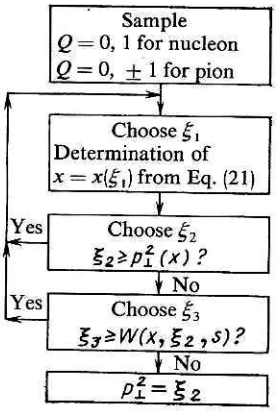

FIG. 26. Algorithm for sampling of x and $p_\perp$ values.

imposed on the characteristics of the two last particles with allowance for the energy–momentum and electric-charge conservation laws (Refs. 1 and 2).[10]

A shortcoming of the method is the frequent rejection of sampled events in the region of large $p_\perp$ due to the very rapid (power-law or exponential) decrease of the distributions $W(x, p_\perp, s)$ with increasing $p^2_\perp$.

The calculation can be done more economically by using the weight functions

$$\mu(x, p_\perp, s) = \begin{cases} \left(E\frac{d^3\sigma(x, 0, s)}{dp^3}\right)_{\text{c.c}} (1-|x|)^{fp^2_\perp} p_\perp^{-2d}, & |x| \leqslant 0.7, \\ \left(E\frac{d^3\sigma(x, 0, s)}{dp^3}\right)_{\text{frag}} \exp\left[Rp^2_\perp/|x|\right], & |x| > 0.7, \end{cases} \tag{22}$$

where $R = R_A$ and $R = R_2$ for the conserved and nonconserved fragmentation particles, respectively, and

$$\mu(x, p_\perp, s) = \left(E\frac{d^3\sigma(x, 0, s)}{dp^3}\right)_{\text{c.nc.}} e^{-1.3p^2_\perp} p_\perp^{-2} \tag{23}$$

for the remaining nonconserved particles. The values of the constants R, f, and d are given in Tables II and XI. The change that must then be introduced into the algorithm (see Fig. 26) is the sampling of the random number ξ_2 in accordance with the distribution $\mu(x, p_\perp, s)$ and application of Neumann's method to the function $W(x, p_\perp, s)/\mu(x, p_\perp, s)$. Since the function μ is simpler than the function W (in the choice of the numbers ξ_2 and ξ_3, the variable x remains fixed), the rejection process is significantly accelerated.

The method described here is very helpful for simulating inelastic "stars" observed in chambers and photographic emulsion and in connection with the analysis of different methodological questions (criteria for selecting definite types of events, efficiency of scanning, debugging of programs for analyzing the results of measurements, etc.). The same methods of analysis as for experimental data can be directly applied to generated "stars" recorded on an appropriate carrier.

[9] If a large number of events are simulated, to accelerate the calculation it is convenient to compile in advance a table of the values of the left-hand sides of Eq. (21) for given values of x and to use it later for the inverse (by interpolation) determination of x from given ξ_1. The algorithm for simulating an inelastic hadron–hadron interaction event in FORTRAN is given in its entirety in Ref. 87.

[10] If the sampled characteristics are not changed, then on the average, for a large number of interactions, the conservation law is satisfied fairly well, but in individual collisions the deviations are very large.

CONCLUSIONS

It must be stressed that all the quantitative and qualitative conclusions about the properties of high-energy πN and NN interactions are not the result of theory but are deduced from phenomenological analysis of the experimental data. Although the original data are very varied, their unification by means of a single approximation makes it possible to obtain a fairly complete picture of the inelastic collision of two hadrons. In particular, the approximations given above contain all the information on the multiplicity and the angular, energy, and momentum distributions collected together in Refs. 39, 48, 80, 85, and 88.

Our calculations have shown that in the regions in which detailed experimental data are currently available the expressions (1)–(6) describe the results of the measurements to within limits close to the averaged experimental errors. The agreement is much less good where there are only scattered and patchy measurements. Finally, in the regions in which no experiments have yet been made at all (for example, at very large s) only a description in order of magnitude can be expected.

Further refinement in the description of the inelastic event requires the resonance channels to be taken into account.[89] It is well known that an appreciable fraction of the secondary particles is produced by the decay of the resonances ρ, ω, etc., which can be calculated very accurately, so that explicit separation of the cross sections $d^3\sigma_{\text{res}}/\text{dp}^3$ of the resonance channels will make it possible to improve the approximation of the observed cross sections $d^3\sigma/dp^3$.

The approximating expressions that we have used are based on general properties of the amplitudes of strong interactions and therefore apply to all types of inelastic hadron–hadron interactions, in particular, to collisions of strange particles and antinucleons with nucleons. This last case is currently of particular interest, since the recently commissioned collider at CERN makes it possible to investigate $p\bar{p}$ collisions at the record accelerator energy $T \simeq 2 \cdot \mathscr{T}^2/M \simeq 150$ TeV ($\mathscr{T} \approx 270$ GeV is the kinetic energy of the colliding particles, and M is their mass).

We should like to use this opportunity to express our thanks to M. G. Meshcheryakov for discussing details of hadron–hadron interactions. We are also grateful to S. Yu. Shmakov, who pointed out possibilities for increasing the efficiency of the Monte Carlo programs, to V. G. Grishin for reading the draft and making many helpful comments, and to N. V. Mokhov and I. L. Azhgireĭ for collaboration.

[1]V. S. Barashenkov, K. K. Gudima, and V. D. Toneev, Acta Phys. Pol. **36**, 415 (1969).
[2]V. S. Barashenkov and V. D. Toneev, Vzaimodeĭstviya vysokoénergeticheskikh chastits i atomnykh yader s yadrami (Interactions of High Energy Particles and Nuclei with Nuclei), Atomizdat, Moscow (1972).
[3]A. A. Logunov, M. A. Mestvirishvili, and Nguyen Van Hieu, Phys. Lett. **25B**, 611 (1967); in: Topical Conf. on High Energy Collisions of Hadrons, Geneva (1968), p. 74.
[4]S. N. Ganguli and D. P. Roy, Phys. Rep. **67**, 201 (1980).
[5]R. D. Field and G. C. Fox, Nucl. Phys. **B80**, 367 (1974).
[6]E. Byckling and K. Kajantie, Particle Kinematics, Wiley, New York (1973) (Russian translation published by Mir, Moscow (1975)).
[7]M. J. Mück *et al.*, DESY Report F1-72/1 (1972); M. G. Albrow *et al.*, in: Proc. of the 16th Intern. Conf. on High Energy Physics, Batavia (1972), p. 940; J. V. Allaby *et al.*, in Proc. of the Fourth Intern. Conf. on High Energy Collisions, Oxford (1972), p. 85; H. J. Sing *et al.*, Nucl. Phys. **B140**, 189 (1978).
[8]M. G. Albrow *et al.*, Nucl. Phys. **B108**, 1 (1976).
[9]J. Whitmore *et al.*, Phys. Rev. D **11**, 3124 (1975).
[10]J. Engler *et al.*, Nucl. Phys. *B* 84, 70 (1975).
[11]V. A. Kobzev *et al.*, Zh. Eksp. Teor. Fiz. **41**, 747 (1961) [Sov. Phys. JETP **14**, 538 (1962)].
[12]T. Vishki *et al.*, Zh. Eksp. Teor. Fiz. **41**, 1069 (1961) [Sov. Phys. JETP **14**, 763 (1962)].
[13]J. Hanlon *et al.*, Phys. Rev. D **20**, 2135 (1979).
[14]M. Csejthey-Barth, Nuovo Cimento **32**, 545 (1964).
[15]G. Alexander *et al.*, Phys. Rev. **154**, 1284 (1967).
[16]G. N. Akerlif *et al.*, Phys. Rev. D **3**, 645 (1971).
[17]Y. K. Lim, Nuovo Cimento **28**, 1228 (1963).
[18]H. Boggild *et al.*, Nucl. Phys. **B27**, 1, 85 (1971).
[19]H. J. Mück *et al.*, Phys. Lett. **B39**, 303 (1972).
[20]F. T. Dao *et al.*, NAL-Pub-74/38-Exp, Batavia (1974).
[21]F. T. Dao *et al.*, Phys. Rev. Lett. **30**, 1151 (1973).
[22]M. Antinucci *et al.*, Lett. Nuovo Cimento **6**, 121 (1973).
[23]G. Damgaard and K. H. Hansen, Contribution to the 16th Intern. Conf. on High Energy Physics, Batavia (1972).
[24]V. Blobel *et al.*, Nucl. Phys. **B69**, 454 (1974).
[25]H. Bluminfeld *et al.*, Phys. Lett. *B* 45, 525 (1973).
[26]M. Boratav *et al.*, Nucl. Phys. **B111**, 529 (1976).
[27]D. R. Ward *et al.*, Phys. Lett.**B62**, 237 (1976).
[28]J. W. Chapman *et al.*, Phys. Lett. **B47**, 465 (1973).
[29]K. Jaeger *et al.*, Phys. Rev. D **11**, 2405 (1975).
[30]J. Engler *et al.*, Nucl. Phys. **B84**, 70 (1975).
[31]T. Kafka *et al.*, Phys. Rev. D **19**, 76 (1979).
[32]A. A. Seidl *et al.*, Bull. Am. Phys. Soc. **19**, 467 (1977).
[33]J. Erwin *et al.*, Phys. Rev. Lett. **32**, 254 (1974).
[34]G. Charlton *et al.*, Phys. Rev. Lett. **29**, 515 (1972).
[35]H. P. Bogachev *et al.*, Zh. Eksp. Teor. Fiz. **38**, 1346 (1960) [Sov. Phys. JETP **11**, 968 (1960)].
[36]Wang Shu Fen, Zh. Eksp. Teor. Fiz. **39**, 957 (1961) [Sov. Phys. JETP **12**, 663 (1961)].
[37]M. Koshiba *et al.*, Suppl. Nuovo Cimento **1**, 1091 (1963).
[38]A. De Marko Trabucco *et al.*, Nucl. Phys. **60**, 209 (1964).
[39]V. S. Barashenkov *et al.*, Fortschr. Phys. **14**, 357 (1966); **15**, 435 (1967); A. K. Likhoded and P. V. Shlyapnikov, Usp. Fiz. Nauk **124**, 3 (1978) [Sov. Phys. Usp. **21**, 1 (1978)]; V. G. Grishin, Inklyuzivnye protsessy v adronnykh vzaimodeĭstviyakh pri vysokikh énergiyakh (Inclusive Processes in Hadron Interactions at High Energies), Energoizdat, Moscow (1982).
[40]Zh. S. Takibaev and É. Boos, Neuprugie vzaimodeĭstviya nuklonov pri vysokikh énergiyakh (Inelastic Interactions of Nucleons at High Energies), Nauka, Alma Ata (1974).
[41]N. A. Dobrotin *et al.*, Nucl. Phys. **35**, 152 (1962).
[42]K. Rybicki, Nuovo Cimento **49**, 233 (1967).
[43]A. A. Kamal and G. K. Rao, Nucl. Phys. **B2**, 135 (1967).
[44]G. Donaldson *et al.*, Phys. Lett. **B73**, 375 (1978).
[45]Y. Eisenberg *et al.*, Nucl. Phys. **B154**, 329 (1979).
[46]V. A. Kobzev *et al.*, Zh. Eksp. Teor. Fiz. **41**, 747 (1961) [Sov. Phys. JETP **14**, 538 (1962)].
[47]G. Charlton *et al.*, Phys. Rev. Lett. **29**, 1759 (1972).
[48]V. S. Murzin and L. I. Sarycheva, Kosmicheskie luchi i ikh vzaimodeĭstvie (Cosmic Rays and their Interaction), Atomizdat, Moscow (1968).
[49]A. M. Rossio *et al.*, Nucl. Phys. **B84**, 269 (1975).
[50]I. N. Vardanyan *et al.*, Preprint R1-12691 [in Russian], JINR, Dubna (1979).
[51]V. V. Ammosov *et al.*, Nuovo Cimento **A40**, 237 (1977).
[52]M. Dentschman, in: Amsterdam Intern. Conf. on Elementary Particles, Amsterdam (1971), p. 153.
[53]T. Ferbel, Report UR-408 Rochester Univ. (1973).
[54]A. U. Abdurakhimov *et al.*, Yad. Fiz. **18**, 545 (1973) [Sov. J. Nucl. Phys. **18**, 281 (1973)].
[55]N. G. Birger *et al.*, Zh. Eksp. Teor. Fiz. **41**, 1461 (1961) [Sov. Phys. JETP **14**, 1043 (1962)].
[56]V. B. Lyubimov *et al.*, Preprint R-974 [in Russian], JINR, Dubna (1962).
[57]M. S. Aĭnutdinov *et al.*, Zh. Eksp. Teor. Fiz. **44**, 413 (1963) [Sov. Phys.

JETP **17**, 282 (1963)].
[58]J. W. Elbert *et al.*, Nucl. Phys. **B19**, 85 (1970).
[59]A. U. Abdurakhimov *et al.*, Yad. Fiz. **17**, 1235 (1973) [Sov. J. Nucl. Phys. **17**, 644 (1973)].
[60]M. E. Binkley *et al.*, Phys. Lett. **B45**, 295 (1973).
[61]D. Bogert *et al.*, Phys. Rev. Lett. **31**, 1271 (1973).
[62]E. L. Berger *et al.*, Nucl. Phys. **B77**, 365 (1974).
[63]D. Fong *et al.*, Phys. Rev. Lett. **37**, 736 (1976).
[64]J. E. Elias, Fermilab-Pub-79/47-Exp., Batavia (1979).
[65]N. S. Angelov *et al.*, Yad. Fiz. **25**, 591 (1977) [Sov. J. Nucl. Phys. **25**, 315 (1977)].
[66]S. Batskovich *et al.*, Yad. Fiz. **27**, 1225 (1978) [Sov. J. Nucl. Phys. **27**, 648 (1978)].
[67]E. L. Berger *et al.*, Report CERN/D. Ph./Phys. 74-27, Geneva (1974).
[68]D. Bogert *et al.*, Report NAL-Conf.-74/55-Exp., Batavia (1974).
[69]S. Hagopian *et al.*, Report FSU HEP 76-12, Florida (1976).
[70]A. Bigi *et al.*, in: Proc. of the 11th Intern. Conf. on High Energy Physics, CERN (1962), p. 247.
[71]T. Ferbel and H. Taft, Nuovo Cimento **28**, 1214 (1963).
[72]S. J. Coldsack, *et al.*, Nuovo Cimento **23**, 941 (1962).
[73]M. I. Ferrero *et al.*, Nuovo Cimento **27**, 1066 (1963).
[74]G. Grote *et al.*, in: Proc. of the 11th Intern. Conf. on High Energy Physics, CERN (1962), p. 64.
[75]É. G. Boos *et al.*, in: Materialy 12-ĭ mezhdunarodnoĭ konferentsii po fizike vysokikh énergiĭ (Proc. of the 12th Intern. Conf. on High Energy Physics), Dubna (1964), p. 156.
[76]G. Heider, Report, Institut für Radiumforschung und Kernphysik, Vienna (1963).
[77]J. R. Elliot *et al.*, in: Proc. of the 17th Intern. Conf. on High Energy Physics, London (1974), p. 162.
[78]N. N. Biswas *et al.*, *ibid.*, p. 761.
[79]N. S. Angelov *et al.*, Yad. Fiz. **23**, 365 (1976) [Sov. J. Nucl. Phys. **23**, 190 (1976)].
[80]M. E. Law *et al.*, "Compilation of data on inclusive reactions," LBL-80, Berkeley (1972).
[81]N. S. Angelov *et al.*, Preprint 1-8064 [in Russian], JINR, Dubna (1974).
[82]A. Sh. Gaĭtinov *et al.*, Yad. Fiz. **24**, 350 (1976) [Sov. J. Nucl. Phys. **24**, 183 (1976)].
[83]I. Ya. Chasnikov, Preprint 1-10696 [in Russian], JINR, Dubna (1977).
[84]A. I. Anoshin *et al.*, Preprint 1-10804 [in Russian], JINR, Dubna (1977).
[85]L. A. Didenko, V. S. Murzin, and L. I. Sarycheva, Asimmetriya adronnykh vzaimodeĭstviĭ (Asymmetry of Hadron Interactions), Nauka, Moscow (1981).
[86]M. Basile *et al.*, Lett. Nuovo Cimento **32**, 321 (1981); Report EP/81-86, CERN (1981).
[87]N. V. Slavin, Preprint B1-2-82-744 [in Russian], JINR, Dubna (1982).
[88]V. S. Murzin and L. I. Sarycheva, Mnozhestvennye protsessy pri vysokikh énergiyakh (Multiparticle Production Processes at High Energies), Atomizdat, Moscow (1974).
[89]N. S. Amelin, V. S. Barashenkov, and N. V. Slavin, Preprints R2-83-656, R2-83-769 [in Russian], JINR, Dubna (1983); E2-84-236 [in English], Dubna (1984).

Translated by Julian B. Barbour